

# The Long-Term Dynamics of Dactyl's Orbit

J.-M. Petit

*Centre National de la Recherche Scientifique, Observatoire de Nice, B.P. 4229, 06304 Nice, France, and Lunar and Planetary Laboratory, University of Arizona, Tucson, Arizona 85721*  
E-mail: petit@obs-nice.fr

and

Daniel D. Durda, Richard Greenberg, T. A. Hurford, and P. E. Geissler

*Lunar and Planetary Laboratory, University of Arizona, Tucson, Arizona 85721*

Received February 21, 1997; revised May 12, 1997

---

Asteroid Ida's satellite Dactyl was observed over  $5\frac{1}{2}$  hr by the Galileo spacecraft imaging system. The observed motion fits a family of orbits parameterized by the mass of Ida. We have tested the stability of these orbits by numerically integrating motion about a realistically shaped model for Ida. Those with pericenter distance  $q \lesssim 65$  km (corresponding to Ida's density  $\approx 3.1$  g cm $^{-3}$ ) are unstable over time scales of a few days to a few months, placing a strong upper limit on Ida's density. Moreover, at the opposite extreme of density, orbits corresponding to densities less than 2.3 g cm $^{-3}$  are chaotic and become unstable after about 1000 years. For density between 2.3 and 2.5 g cm $^{-3}$ , Galileo family orbits are chaotic but there is no indication of instability over thousands of years. Dactyl likely formed at the same time as Ida, so its orbit must be stable over time scales much longer than we have been able to explore numerically. As a start toward understanding long-term stability, we have investigated the character of orbits commensurate with the rotation of Ida within the Galileo family. We found that the overlap of high-order resonances for low densities of Ida explains the chaotic behavior of orbits. The low-order  $p:1$  and  $p:2$  resonances, corresponding to a high density for Ida, are distinct and stable and are all consistent with the longitudinal position of Dactyl at the epoch of the Galileo encounter. However, there is no evidence of preferential stability of resonant orbits against collision with Ida or escape over 6000 years. If a resonant orbit is actually occupied, it may have been selected by a longer-term stability or by dissipative processes. © 1997

Academic Press

## I. INTRODUCTION

Asteroid 243 Ida's satellite Dactyl was discovered in imaging data returned by the Galileo spacecraft after its August 28, 1993, encounter with the asteroid (Belton and Carlson 1994). Because Galileo was targeted to fly by Ida

at too great a distance for Doppler data to be useful in determining the asteroid's mass, the discovery provided a fortuitous opportunity to find the mass and mean density of Ida if an orbit for the satellite could be determined. Dactyl appeared in 47 of the returned images taken over  $5\frac{1}{2}$  hr. Unfortunately, Dactyl's plane about Ida was nearly coincident with Galileo's trajectory past the asteroid, so no single orbit could be unambiguously defined from the limited imaging data alone. The observed positions fit any member of a continuous family of Keplerian orbits, each orbit corresponding to a particular assumed mass of Ida (Byrnes and D'Amario, 1994, Belton *et al.* 1995, 1996). We refer to this set as the "Galileo family" of candidate orbits.

Figure 1 shows the semimajor axis, eccentricity, and inclination of the Galileo family orbits as functions of Ida's mass. As can be seen, all orbits have a low inclination of order  $8^\circ$  with respect to Ida's equatorial plane. The Galileo family includes elliptic orbits with eccentricity as low as 0.09, as well as hyperbolic trajectories for the lowest-density cases. The hyperbolic cases may be ruled out based on Hubble Space Telescope searches for Dactyl in the vicinity of Ida after its discovery (Belton *et al.* 1995) and from statistical arguments on the small likelihood of observing a passing asteroid just during the short time of the encounter so close to Ida (Belton *et al.* 1996). Further constraints on the orbit of Dactyl, and thus on the mass and density of Ida, come from dynamical studies of orbital stability. In Section II we describe the dynamical constraints that can be placed on the range of allowable Dactyl orbits that have been found by short-term integration using both a simple triaxial ellipsoidal shape model and a realistic irregular shape model for Ida (Thomas *et al.* 1966). Some of the results of the work reported in Section II have been integrated into descriptions of Ida's properties and history by Belton *et al.* (1995, 1996) and by Greenberg *et al.* (1996).

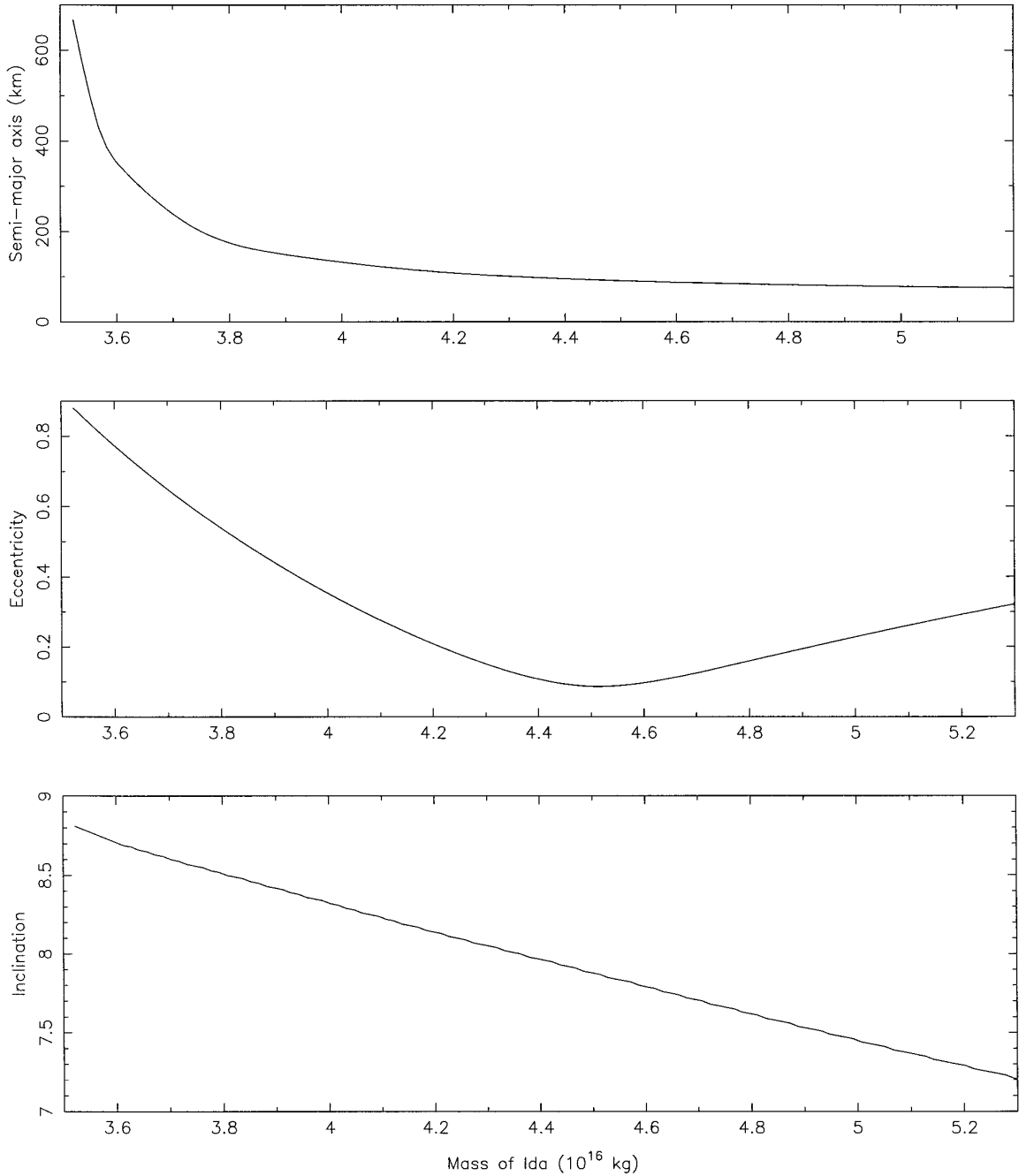


**FIG. 1.** Semimajor axis, eccentricity, and inclination, in degrees (from top to bottom), of the Galileo family orbits as functions of Ida's mass. Here are included only the elliptic orbits with pericenter distance larger than 50 km.

We then present in Section III our study of resonant orbits about a realistically shaped Ida. We first describe how commensurabilities between Dactyl's orbital period and Ida's rotational period can be locked (Section IIIA). Next we search for orbits in the Galileo family that are commensurate with Ida's rotation (Section IIIB) and check (Section

IIIC) that these orbits are consistent with orbital positions from Galileo images. In Section IIID we give a Hamiltonian description of the resonant structure of the Galileo family. The relative stability of resonant orbits and nearby non-resonant orbits is discussed in Section IIIE, and our conclusions are summarized in Section IV.

## II. BOUNDARIES OF ORBITAL STABILITY

To study the stability of orbits around a rapidly rotating, elongated asteroid, we first modeled the primary asteroid as a triaxial ellipsoid with parameters similar to Ida's (Petit *et al.* 1994). With such a primary, at Dactyl's close distance orbits can be quite irregular. Our preliminary numerical integrations showed that the most critical parameter governing stability is the pericenter distance. For low enough pericenter distances, orbits impact the primary or escape within a few hundred periods. For retrograde orbits (motion opposite the sense of rotation), the critical pericenter distance is about 50 km. For prograde orbits (as Dactyl's is), motion is unstable if the pericenter is lower than about 70 km. Such a restriction would rule out a large range of the Galileo family of orbits, allowing only those orbits that correspond to a mass density less than about  $3 \text{ g cm}^{-3}$  (Petit *et al.* 1994, Belton *et al.* 1996).

To test that result, we have systematically examined the stability of Galileo family orbits. This series of numerical experiments used the triaxial ellipsoid reported by Thomas *et al.* (1996), as the best fit to Ida's figure, with axes 59.8, 25.4, and 18.6 km. The potential of the triaxial ellipsoid is then given by elliptical integrals (Chauvineau *et al.* 1993). We used a Bulirsch and Stoer integrator, with self-adaptive time steps, and required a relative precision of  $10^{-10}$  at each time step. The precision was actually about  $10^{-12}$  to  $10^{-13}$  for each time step, and even after more than a million orbits, the Jacobi constant had changed by only  $10^{-8}$  in relative value.

We found that along the continuum of orbits that can fit the Galileo images, prograde orbits with a pericenter distance  $\leq 65$  km exhibit strong short-term instabilities. They either impact Ida or escape the asteroid in only a few hours to days. Here we define escape as a positive binding energy when the distance from Ida is greater than 500 km. All significant changes in energy occur near pericenter. At large distances, the rotation of Ida averages out its effect on energy.

Figure 2 shows the results of a numerical integration starting on an osculating orbit from the Galileo family. This initial orbit corresponds to the value of Ida's mass  $M = 5.7 \times 10^{16} \text{ kg}$  ( $\rho = 3.54 \text{ g cm}^{-3}$ ), and has semimajor axis  $a = 70.07 \text{ km}$  and pericenter distance  $q = 40.46 \text{ km}$ . The satellite makes five revolutions before impacting Ida after less than 37 hr. Figure 3 illustrates a slightly longer-lived escaping case,  $M = 5.1 \times 10^{16} \text{ kg}$  ( $\rho = 3.17 \text{ g cm}^{-3}$ ), with  $a = 75.96 \text{ km}$  and  $q = 56.18 \text{ km}$ . Between close approaches, the energy oscillates around a constant value (Fig. 3b). At each passage at pericenter, the energy gets an impulse and changes by a potentially large amount. The satellite has four close encounters with Ida and during the last one, after 29 days in orbit, received enough energy to escape. Figure 4 shows the case for  $M = 4.8 \times 10^{16} \text{ kg}$

( $\rho = 2.98 \text{ g cm}^{-3}$ ), with  $a = 81.43 \text{ km}$  and  $q = 68.55 \text{ km}$ . The orbital energy remains constant and stable, except for oscillations due to the rotation of Ida, showing no signs of impending instability over the 100-day time scale of the integrations. Our numerical experiments show that, with this ellipsoidal-Ida model, orbits in the Galileo family that correspond to assumed  $M > 4.93 \times 10^{16} \text{ kg}$  ( $\rho > 3.06 \text{ g cm}^{-3}$ ,  $q < 63 \text{ km}$ ) are highly unstable on a time scale of  $\sim 100$  days. Those orbits corresponding to smaller values of  $M$  are generally stable for as long as we ran the integrations (1000 years or more).

Scheeres *et al.* (1996) have analytically discussed how escape can occur, but only considering up to second-order harmonics in the gravitational field. That discussion helps give insight into the mechanics. However, Ida is so irregular that higher-order harmonics are significant.

We next explored the influence of the irregular shape of Ida on the short-term instability limits. We approximate the shape model for Ida (Thomas *et al.* 1996) by a collection of 44 packed spheres of different sizes. By choosing the number, masses, and arrangement of spheres we obtained a body with nearly the same gravitational potential as a uniform density in the Thomas *et al.* model figure while minimizing the time necessary to compute the gravitational force during numerical integration. The difference between our 44-sphere model and the shape model of Thomas *et al.* is less than the uncertainty in the true gravitational field.

With this representation of the real shape, the fate of individual orbits is somewhat different from what we found in the triaxial-ellipsoid case, and the boundary between instability (impact or escape) and stability is changed slightly. Figure 5 shows, for the realistic shape model, the same initial orbit as Fig. 2. The satellite escapes after less than 1 year in orbit. To determine more precisely the boundary between stable and unstable orbits, we interpolated osculating elements from those tabulated for the Galileo family by Belton *et al.* (1996). For our 44-sphere model, the limit of stability for the Galileo family of candidate orbits is at  $M = 4.99 \times 10^{16} \text{ kg}$  ( $\rho = 3.10 \text{ g cm}^{-3}$ ,  $a = 78 \text{ km}$ ,  $q = 60 \text{ km}$ ). Again, orbits below the limit are stable for at least  $\sim 1000$  years, while those for larger  $M$  impact Ida or escape in  $\leq 100$  days, or a few hundred orbits (see Fig. 6).

Next we consider the stability of the orbits with large values of  $e$ , just below the hyperbolic limit ( $e = 1$ ). We find that these orbits are very stable on the short time scales that characterized the instabilities near the upper limit of  $M$ . However, numerical integrations over a few thousand years do show both unstable and chaotic behavior.

For those numerical experiments, we followed both the behavior of the orbital elements and the Lyapunov characteristic number, which serves as an indicator of chaos (see

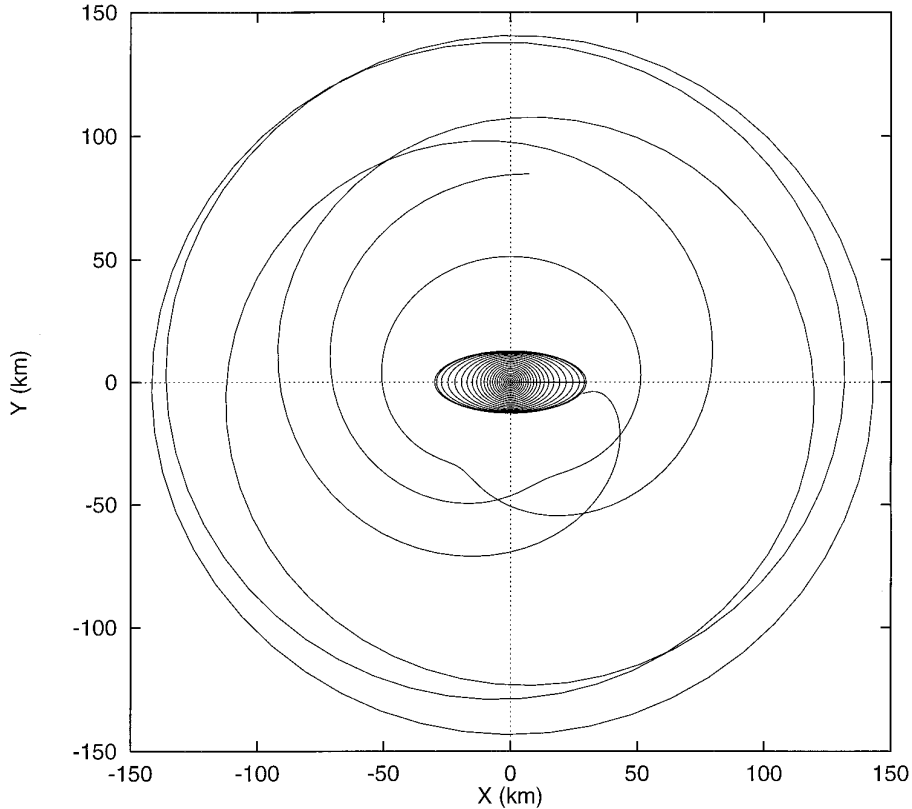


**FIG. 2.** An orbit that is unstable ending in impact on the primary in less than a few days. Orbit is plotted in the frame rotating with Ida. The central ellipse represents the projection of the primary (a triaxial ellipsoid best fit to Ida's figure) on the  $(x, y)$  plane, with mass  $M = 5.7 \times 10^{16}$  kg, near the large-mass end of the Galileo family.

Appendix). We found that for the Galileo family of orbits, those with  $M \lesssim 4.0 \times 10^{16}$  kg ( $e \gtrsim 0.36$ ) are chaotic; the Lyapunov characteristic indicator levels off after  $\lesssim 100$  years. However, a chaotic orbit is not necessarily unstable; it could be long-lived. An example of a chaotic system with well-bounded, regular behavior and an indefinite lifetime is the system of terrestrial planets (Laskar 1990).

In our case, orbits with  $M \leq 3.65 \times 10^{16}$  kg are chaotic, leading to eventual satellite escape. Figure 7a shows the time evolution of the Lyapunov characteristic indicator for  $M = 3.6 \times 10^{16}$  kg. The orbit is clearly chaotic. Moreover, long after chaos was evident (a few years in Fig. 7a), the satellite reached an escaping orbit: the semimajor axis and eccentricity follow a kind of random walk with a slight tendency to increase. This results in a decrease of the “averaged pericenter distance” defined by  $q = a(1 - e)$ , where  $a$  and  $e$  are the values at apocenter (Fig. 7b). When this pericenter distance reaches 74 km, orbital change accelerates. This occurs when  $e$  is about 0.9 and  $a$  is 740 km. After a few more revolutions (about 230 years after the start of integration), the satellite reaches a hyperbolic orbit and escapes.

On the other hand, the orbit for  $M = 3.75 \times 10^{16}$  kg, even though chaotic, seems to be stable over the 3000 years of integration. Figure 8a shows the time evolution of the Lyapunov characteristic indicator, which levels off at a value of the order of  $10^{-8.1}$  after some 30 years. Despite this formal “chaos,” the osculating elements seem to be trapped in a finite region not connected with the region of escaping orbits. Figure 8b shows the time evolution of the semimajor axis. Although chaotic, its range of variation is limited to 430 m around a value of 189.98 km. Similarly, its eccentricity has a value of  $0.5693 \pm 0.0007$ . There is no hint of instability.

None of the Galileo family orbits given by Belton *et al.* (1996) with  $4.0 \times 10^{16}$  kg  $\lesssim M \lesssim 4.99 \times 10^{16}$  kg showed a sign of instability over the 3000-year of integration. Nor are they chaotic: their Lyapunov characteristic indicator decreases regularly with time (e.g., Fig. 9).

The boundaries for stable orbits found from these integrations are indicated in Fig. 6, where the Galileo family of candidate orbits is also shown. The range of stable but chaotic orbits is  $3.65 \times 10^{16}$  kg  $< M < 4.0 \times 10^{16}$  kg. The total range of stable orbits is  $3.65 \times 10^{16}$  kg  $< M <$

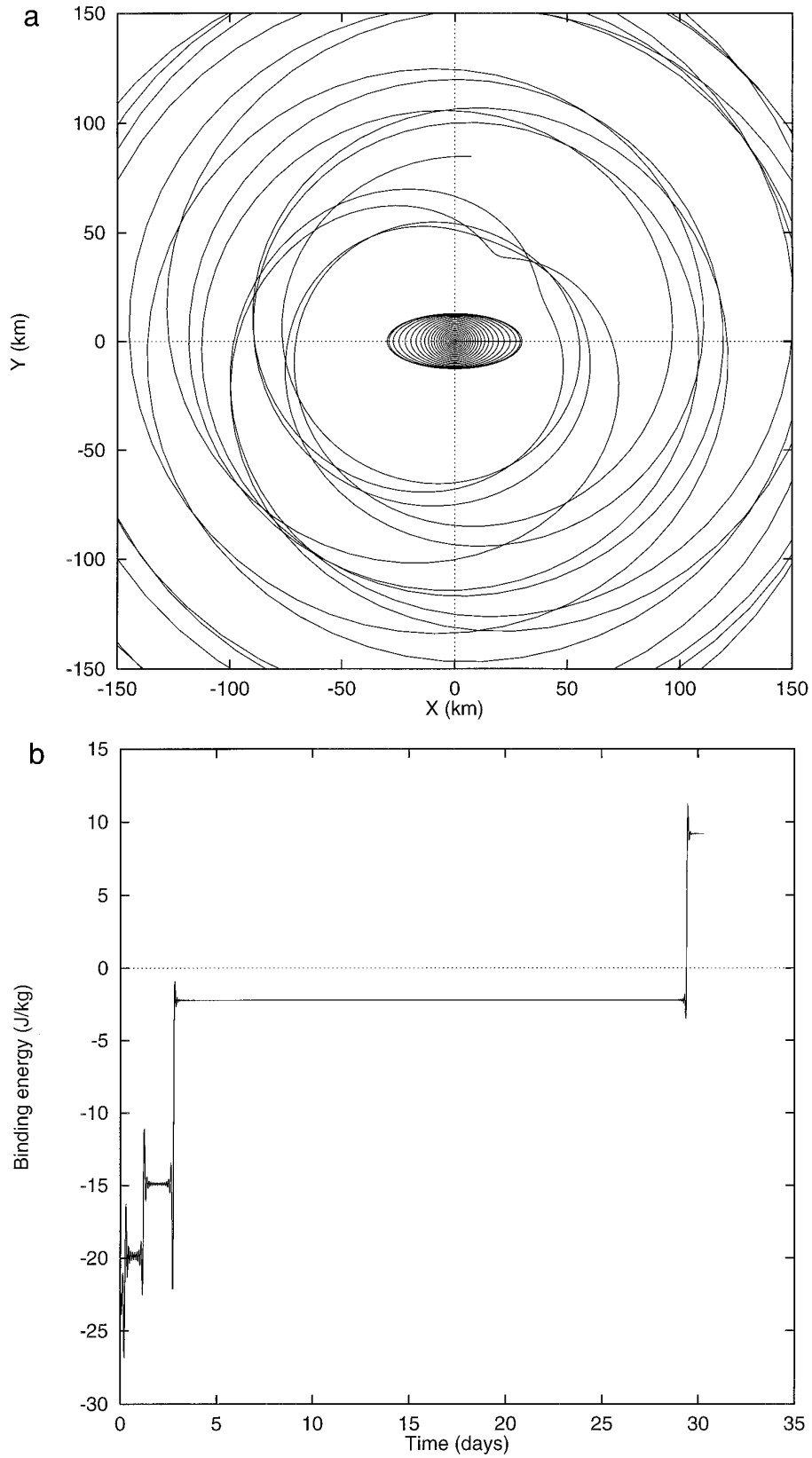


**FIG. 3.** (a) Same as Fig. 2 for  $M = 5.1 \times 10^{16}$  kg. (b) Time evolution of energy per unit mass of the satellite for the same case as (a). Negative energy corresponds to a bounded orbit, positive energy to a hyperbolic trajectory. This orbit leads to rapid escape.

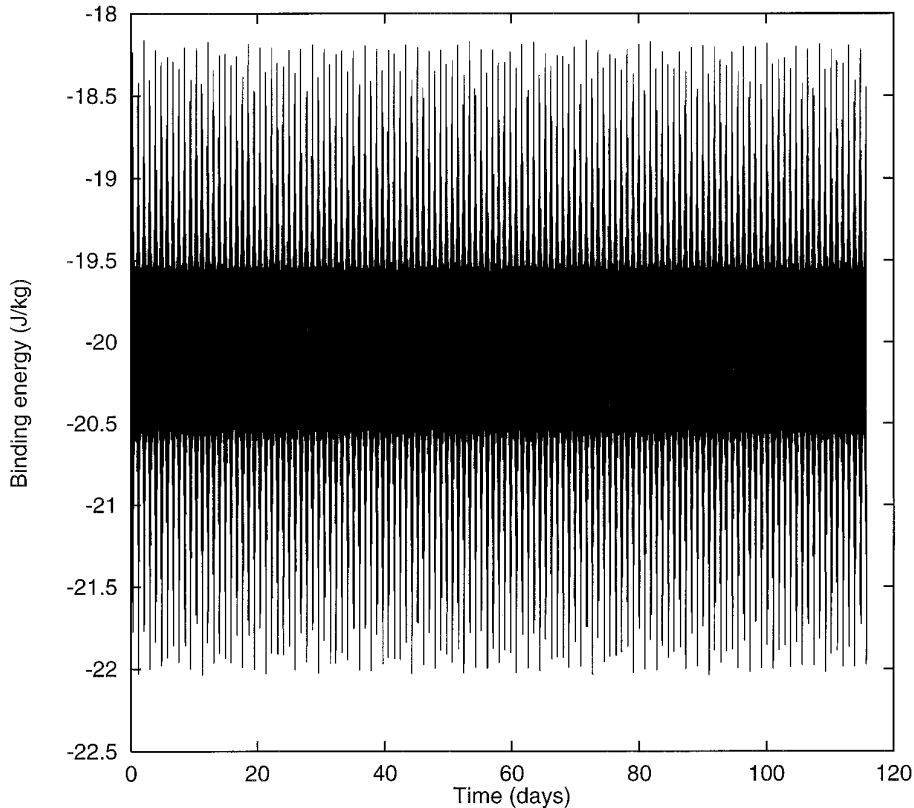


FIG. 4. Same as Fig. 3b for  $M = 4.8 \times 10^{16}$  kg. Such an orbit is stable for at least thousands of years.

$4.99 \times 10^{16}$  kg. Assuming a volume of  $16,100 \text{ km}^3$  (Thomas *et al.* 1996) this mass range yields a mean density  $\rho$  in the range  $2.27$  to  $3.10 \text{ g cm}^{-3}$ .

To attempt to restrict further the range of possible masses we must consider longer-term stability.

### III. STABLE COMMENSURABLE ORBITS

Dactyl was probably created at the same time as Ida (Durda 1996) during the event that formed the Koronis asteroid family as much as 1.5 byr ago (Durda 1993), although it may have suffered major disruptions and size reduction by impactors  $\leq 10^8$  years ago (Greenberg *et al.* 1996). It is also possible that it formed even more recently, e.g., as ejecta from a large cratering event on the asteroid (Durda and Geissler 1996). In any case, it is unlikely that a short-lived satellite would be in orbit just as Galileo encountered Ida. Therefore, we need to understand stability limits over time scales much longer than considered in Section II. Resonant orbits are often especially stable and may play a role in maintaining orbits in Ida's complex dynamical environment. Periodic orbits may extend the range of possible conditions that can lead to a long-lived satellite.

#### A. Character of Stable Commensurabilities

To address that possibility, we first searched for stable, periodic orbits around the triaxial-ellipsoid model of Ida. To reduce the volume of phase space to explore, and because Dactyl's inclination is small, we considered only orbits in Ida's equatorial plane. One class of orbit, prograde, synchronous, and locked to a longitude  $90^\circ$  from the long axis, was thought a priori to be stable. Such an orbit would be in effect trapped in the gravitational harmonic "topography." Numerical integration confirmed that such orbits are stable for moderately elongated primaries. However, we discovered that such orbits proved to be unstable for a triaxial primary as elongated as Ida. Similar results were reported by Scheeres (1994).

For an ellipsoid with Ida's dimensions, we did find a class of stable, highly eccentric, retrograde orbits that are commensurate with Ida's rotation period. This discovery came about in the following way. We found that for motion near (but not exactly at) a  $p:1$  commensurability (where  $p$  is an integer), pericenter longitude precesses through  $360^\circ$ , but pericenter distance  $q = a(1 - e)$  is correlated with the rotational phase of Ida: when pericenter is located near the long axis of Ida, the pericenter distance is greater than average. That observation motivated further investi-

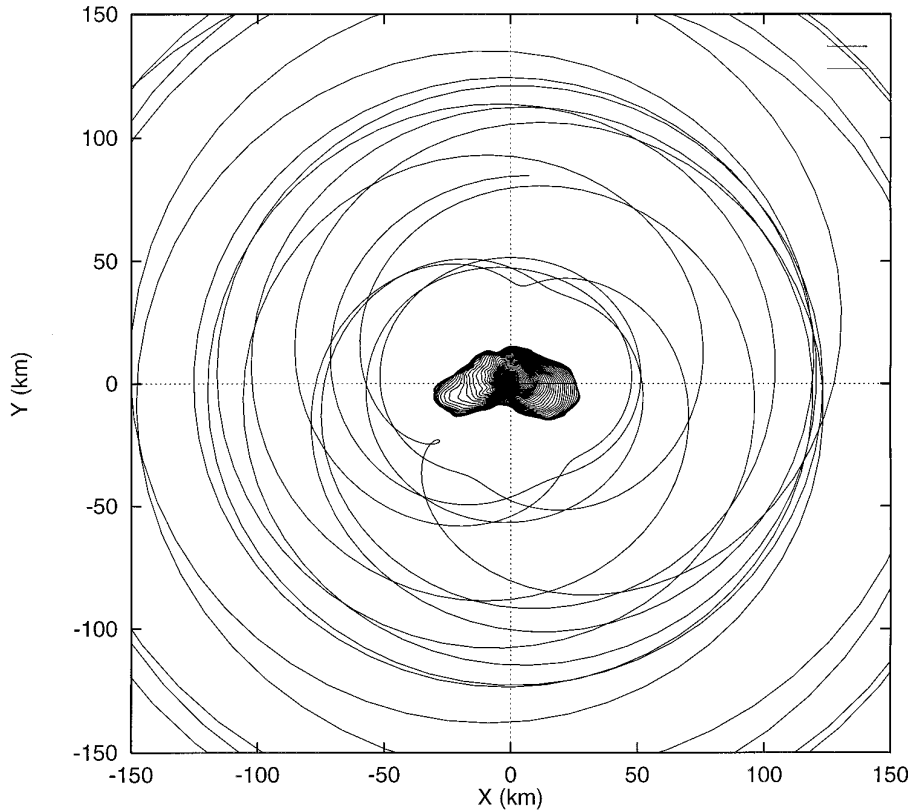


FIG. 5. Same as Fig. 2 for a realistic 44-sphere shape model for the primary. Escape occurs in less than a year.

gation, revealing that orbits could be found that were trapped with pericenter  $90^\circ$  from the long axis. In the case of prograde orbits like Dactyl's, the stability zone does not extend as close to the primary as it would be for retrograde orbits, which can be subject to the same kind of trapping phenomenon. Here we illustrate the phenomenon with a retrograde orbit to show how the protection mechanism works to prevent close encounters between the satellite and the ends of Ida. Retrograde orbits are more stable than prograde ones, and display stronger effects, making it easier to see how the mechanism works. However, the same general process can apply for prograde orbits.

This type of orbit is stabilized because pericenter is always near the shorter axis of Ida. Consider the case shown in Fig. 10a, a 6:1 commensurability. This figure shows four revolutions of a retrograde orbit with pericenter near 48 km. The dots indicate the position of the satellite at times when the primary is oriented as shown (central ellipse). Figure 10b shows that the longitude of pericenter is locked to  $-90^\circ$ . The dots in Fig. 10b correspond to the passage at pericenter. Similar orbits can be found for the 5:1, 7:1, etc., commensurabilities.

Next consider commensurabilities of the form 11:2, 13:2, 15:2, etc. In such cases, the location of pericenter alternates,

first on one side of Ida and then on the other. Numerical integration shows that pericenter longitudes still avoid the long axis, just as for the  $p:1$  cases. Such a retrograde orbit is represented in Fig. 11, which shows the alternating position of pericenter. Even though pericenter can come very close to Ida, the orbit is stable and pericenter is confined far from the long axis so as to protect the satellite from close approach. This kind of orbit stabilization may be able to counteract long-term perturbations, such as solar tides and tidal torques, which might otherwise destabilize orbits on time scales comparable to, or less than, the age of Ida.

The stability locking pericenter away from the long axis is governed by exchanges of energy and angular momentum, especially when the satellite is close to the primary. The lock between the rotational phase of the asteroid and the sub-satellite longitude is maintained by the force due to the mass at the ends of the long axis, which in effect repels pericenter away from the bulge. This effect helps stabilize the orbit.

To understand the underlying physics of this stabilizing interaction between the primary's bulge and an orbiting satellite, we approximate the primary's shape as a set of three spheres: a larger central sphere whose diameter matches the shorter principal axis of Ida, and two smaller

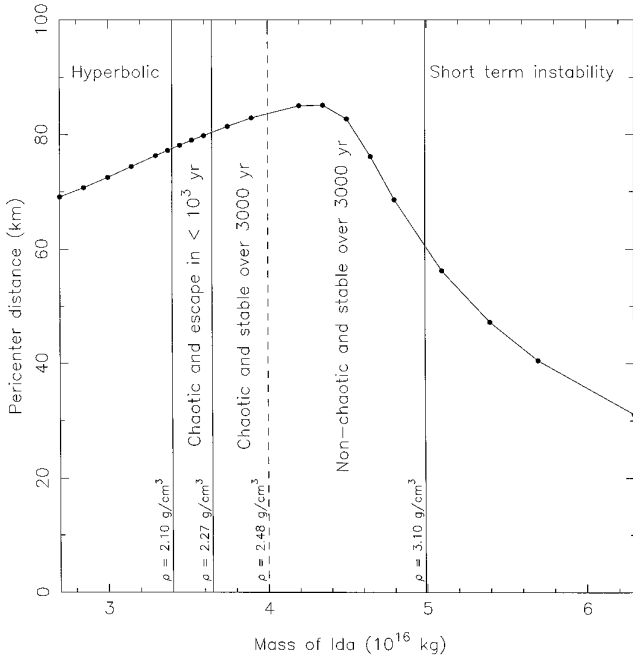


**FIG. 6.** Plot of pericenter distance versus mass of Ida for the Galileo family of orbits (curve). Points are values tabulated by Belton *et al.* (1996). Zones of stability and chaos are indicated. Density of Ida is constrained between 2.3 and 3.1  $\text{g cm}^{-3}$ .

spheres placed opposite each other roughly filling the remainder of Ida's long dimension (central body in Fig. 12a).

When the satellite is about  $45^\circ$  away from the long axis, the torque due to the two small spheres is maximum. (At  $0^\circ$  or  $90^\circ$  the torque would be zero by symmetry.) The torque is stronger close to pericenter than elsewhere along the orbit. Figure 12a shows an orbit at the 5:1 commensurability.

If pericenter were just aligned with the short axis of the primary, then the locations when the satellite is  $45^\circ$  (for example) from the short axis, are symmetrical and the two perturbations cancel each other. On the other hand, if the short-axis longitude is reached after (or before) pericenter, then the perturbation felt for the preceding passage at  $45^\circ$  is stronger (or weaker) than the one felt for the following passage at  $45^\circ$ . We can calculate the perturbing force due to the two long axis bulges (simulated by the two smaller spheres). The resulting orbital energy change rate is shown in Fig. 12b (solid line). (The results for the three-sphere model are confirmed by comparison with a triaxial ellipsoid, shown by the dashed curve in Fig. 12b.) The short-wavelength variations represent the rapid rotation of the primary relative to the direction of the satellite, and the envelope defining the amplitude of the oscillations is centered about pericenter. If (as in the case shown) pericenter does not occur when the satellite is aligned with an axis of symmetry of the primary, the curve is asymmetrical and a net energy change is accumulated.

This change in orbital energy (and, hence, semimajor axis) results in a slight change in the orbital period, causing the time of the next pericenter passage to be slightly advanced or retarded, depending on the phase of pericenter relative to the long axis. This effect tends to return the longitude of pericenter toward a longitude  $90^\circ$  from the long axis. The orbit of such a hypothetical satellite is thus stabilized.

An analytical treatment of the stability mechanism is given by Scheeres *et al.* (1996) for an elongated primary to second order in gravitational harmonics.

Through numerical integrations we have shown that similar stable, synchronous orbits can exist around an Ida-shaped primary as well. Results shown here are for the 44-sphere model, but they have also been confirmed with an alternative model that simulates Ida's figure by 4736 point masses on a uniform grid within the shape defined by Thomas *et al.* (1996). (The integrations are much shorter than those used in Section II to define the limits of orbital stability, making such a model viable.) As with triaxial-ellipsoidal primaries, the pericenter of the satellite's orbit is locked away from Ida's longer axis, although it can be substantially far from the  $90^\circ$  longitude due to Ida's irregular and asymmetric shape. For example, Fig. 13a shows the position of pericenter over a libration period for a 6:1 resonance. Pericenter is locked to a longitude approximately  $55^\circ$  from Ida's long axis. In contrast to orbits around symmetric, ellipsoidal primaries, for  $p:1$  commensurabilities, pericenters are locked only on the convex side of Ida. The asymmetric shape generally prevents orbits from being stable with pericenters on the concave side of the asteroid for low-order resonances. For  $p:2$  commensurabilities, pericenter alternates between longitudes on opposite sides of the asteroid (e.g., Fig. 13b). For all these cases, motion remains within  $1^\circ$  of the equator, and out-of-plane motion introduces only small oscillatory effects on the libration.

### B. Commensurable Orbits That Fit Galileo Observations

The family of Keplerian orbits that fit the Galileo imaging data spans a continuous range of values of semimajor axis  $a$  as discussed in Sections I and II. The range of values found to have short-term stability (Section II) corresponds to a range of orbital periods that includes the following commensurabilities with Ida's period: 5:1, 6:1, ..., 40:1 and 9:2, 11:2, ..., 81:2. The exact value of  $a$  at which an orbit is commensurable depends on the value of  $e$  as well. Therefore we have explored orbital behavior numerically, using the 44-sphere model for Ida's figure (and verifying results with the 4736-sphere model), to identify precisely which orbits in the Galileo family have  $(a, e)$  values that match commensurable orbits (Hurford *et al.* 1995).

For these experiments, initial orbits are in Ida's equatorial plane to reduce the volume of phase space to investi-



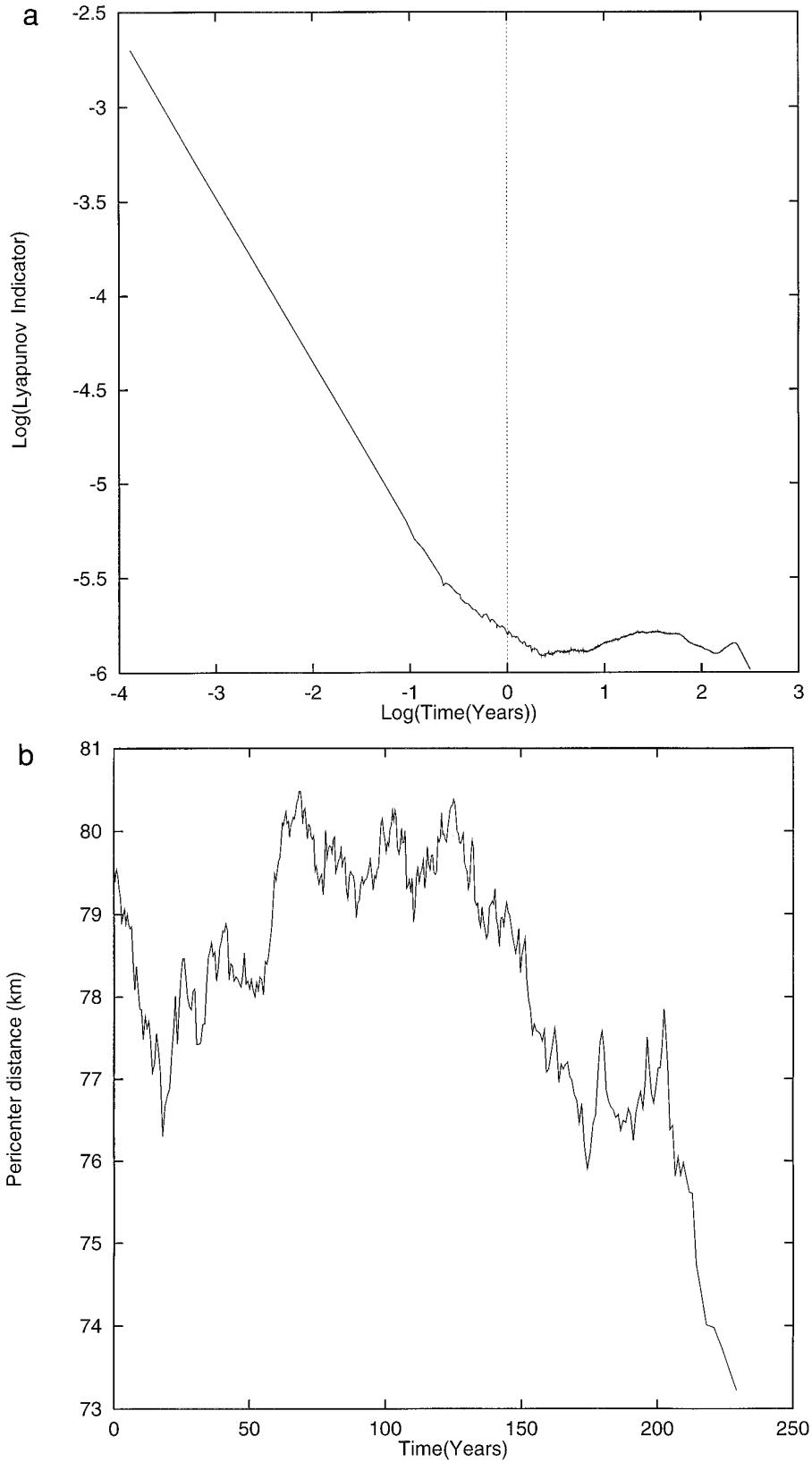


**FIG. 7.** (a) Time evolution of the Lyapunov characteristic indicator for  $M = 3.6 \times 10^{16}$  kg. The orbit is chaotic and the satellite eventually escapes. (b) Time evolution of the “averaged pericenter distance”  $q = a(1 - e)$  where  $a$  and  $e$  are the semimajor axis and eccentricity defined at apocenter. Escape occurs after  $q$  drops below 74 km.

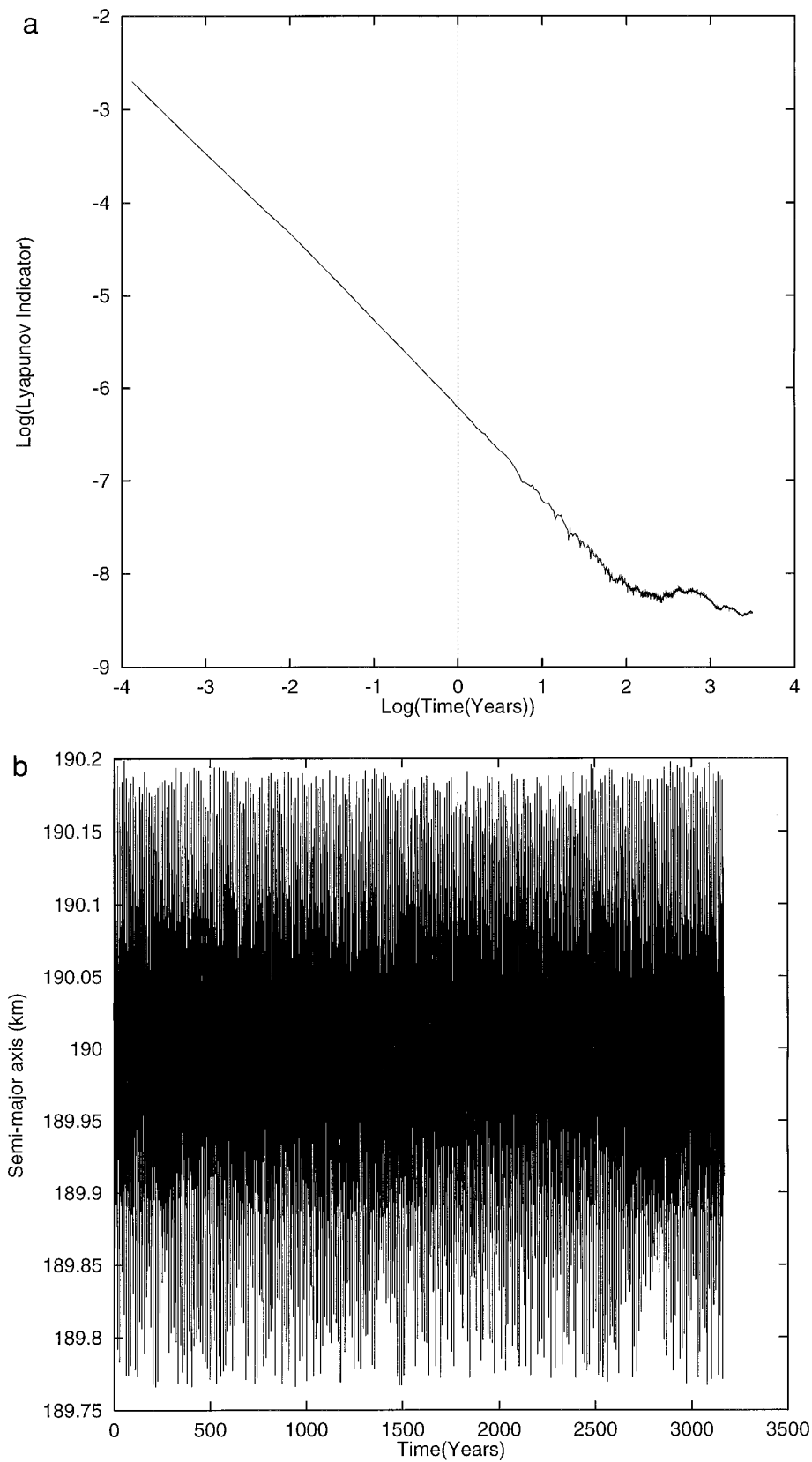


**FIG. 8.** (a) Same as Fig. 7a for  $M = 3.75 \times 10^{16}$  kg. The orbit is chaotic but the satellite does not escape. (b) Time evolution of the semimajor axis at apocenter.

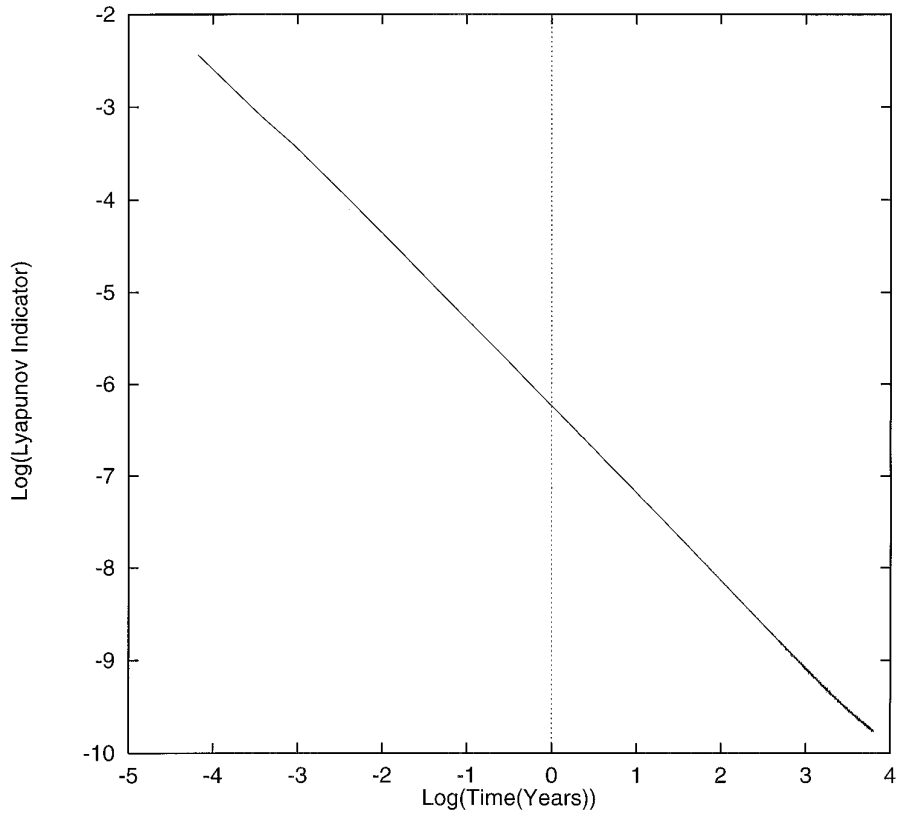


FIG. 9. Same as Fig. 7a for  $M = 4.65 \times 10^{16}$  kg. The orbit is stable for at least 3000 years, with no evidence of chaos.

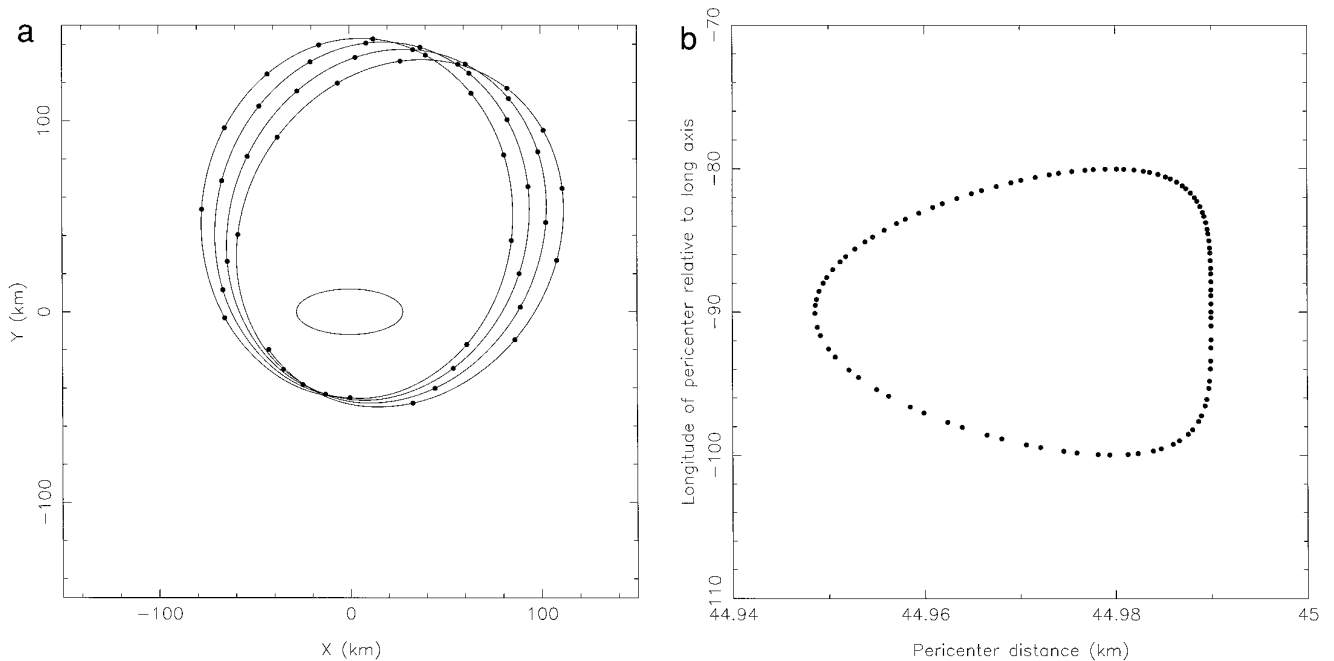


FIG. 10. (a) The 6:1 commensurable retrograde orbit plotted in an inertial frame for an ellipsoidal primary. Dots indicate the position of the satellite when the primary is oriented as shown (central ellipse). This orbit is highly eccentric:  $e \sim 0.47$ . (b) Pericenter longitude relative to primary's long axis versus pericenter distance.

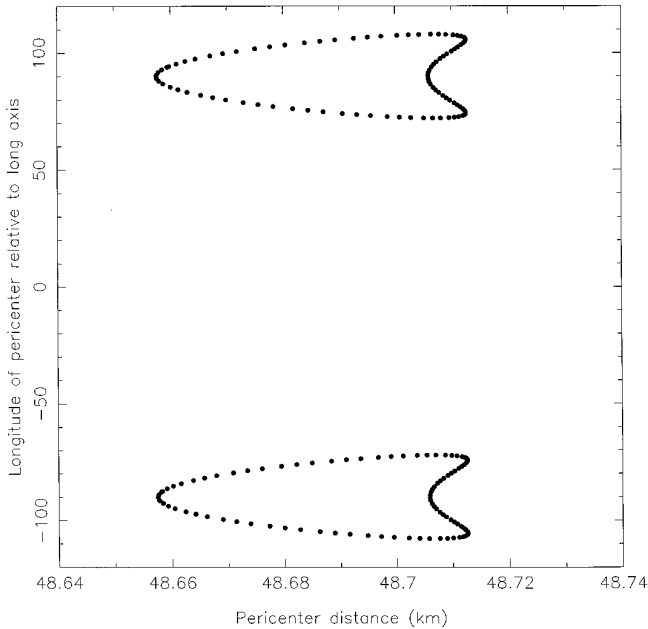


FIG. 11. Same as Fig. 10b for a 13:2 commensurability.

gate. However, the integrations are fully three-dimensional. Despite the irregular shape of Ida, the subsequent inclination never exceeds about a degree. This is not greatly different from Dactyl’s actual inclination of  $\sim 8^\circ$  and many numerical integrations with correctly inclined Galileo family orbits show that the zero-inclination approximation does not affect the results significantly. In this paper, we have also concentrated only on the lower-order resonances (7:1, 13:2, and lower), because higher-order resonances are assumed to be much weaker and therefore of less potential significance in stabilizing the orbit. Also, the higher-order resonances (larger  $a$ ) correspond to lower densities ( $< 2.6 \text{ g cm}^{-3}$ ) for Ida in the Galileo family which would require substantial porosity.

The family of orbits that fit the Galileo images represent a single continuous line through  $(a, e)$  space. Each  $(a, e)$  value corresponds to a particular assumed value for the mass  $M$  of Ida. For each  $M$  value, we searched by a trial-and-error procedure for the stable commensurable orbit that has the same  $e$  value as in the Galileo family. (In fact, as discussed in Section IIIA, for any commensurable orbit,  $e$  oscillates slightly during each orbit, so we matched the average  $e$ .) In general, the average  $a$  over one of these commensurable orbits is not the same as that for the Galileo family orbit with the same  $e$  and  $M$ . In Fig. 14, we show  $a$  as a function of  $M$  for each of the commensurabilities of potential interest. For comparison, we show  $a(M)$  for the Galileo family of possible orbits.

Points in Fig. 14 at which the curves for the resonant orbits intersect the Galileo family orbits represent sets of

$(a, e, M)$  values consistent with the Galileo data as well as with stable commensurable motion.

For the orbital elements defined in that way, we have numerically confirmed that pericenter is locked to a specific longitude on Ida as described in Section IIIA. In fact, the cases shown in Fig. 13 are in the Galileo family as well as commensurable. The Ida-centric longitude of pericenter is shown in Table I as “stable longitude” for commensurability.

### C. Are Orbital Positions from Galileo Images Consistent with Resonant Orbits?

If Dactyl indeed exists on one of these stable, commensurate orbits, not only must the orbital elements  $(a, e)$  of the satellite be consistent with the observations, the orbital position relative to the rotational orientation of Ida must match as well. At the epoch 28 August 1993 16:52:05 UT all Galileo family orbits pass through a reference point  $\sim 90 \text{ km}$  from Ida at longitude  $85^\circ$ , indicated in Fig. 15 (from Belton *et al.* 1995). Several of the Galileo family orbits are shown for a range of discrete values of  $M$  for Ida. Knowing the period and orientation in space of the osculating orbits allows us to advance Dactyl along a given orbit from the reference position at the Galileo reference epoch to the pericenter of that orbit. During the time of travel to pericenter Ida rotates as well (Fig. 16 for the 5:1 case). This procedure gives the Ida-centric longitude of pericenter based on the Galileo observations. Table I shows this value for each commensurable orbit in the Galileo family.

The nominal observed position of Dactyl and orientation of Ida at the Galileo flyby epoch give pericenter at about  $\leq 20^\circ$  of the value for the 9:2 and 5:1 resonances only. The 7:1 resonance could be a stable libration only if the amplitude is  $\geq 80^\circ$  (peak to peak). The other ones would require even larger amplitude, as much as  $320^\circ$  in the case of 6:1.

The position of Dactyl is known with a rather high accuracy, but the orientation of the pericenter is uncertain by approximately  $\pm 10^\circ$  (for  $e \sim 0.2$ , e.g., 9:2 and 7:1) up to  $\pm 35^\circ$  (for  $e \sim 0.1$ , e.g., 6:1). The error on that angle translates into a significant uncertainty in arrival time at pericenter, which in turn gives uncertainty in the Ida-centric longitude of pericenter about five times bigger. Thus any of these low-order resonances is possible within the constraints of the Galileo observations. For any of these resonances the corresponding density of Ida is given in Table I. In the next section we describe the dynamics of resonances more formally and show that the 5:1 commensurable orbit may be most probable. We also discuss whether resonant orbits are more stable than non-resonant ones over longer time scales.

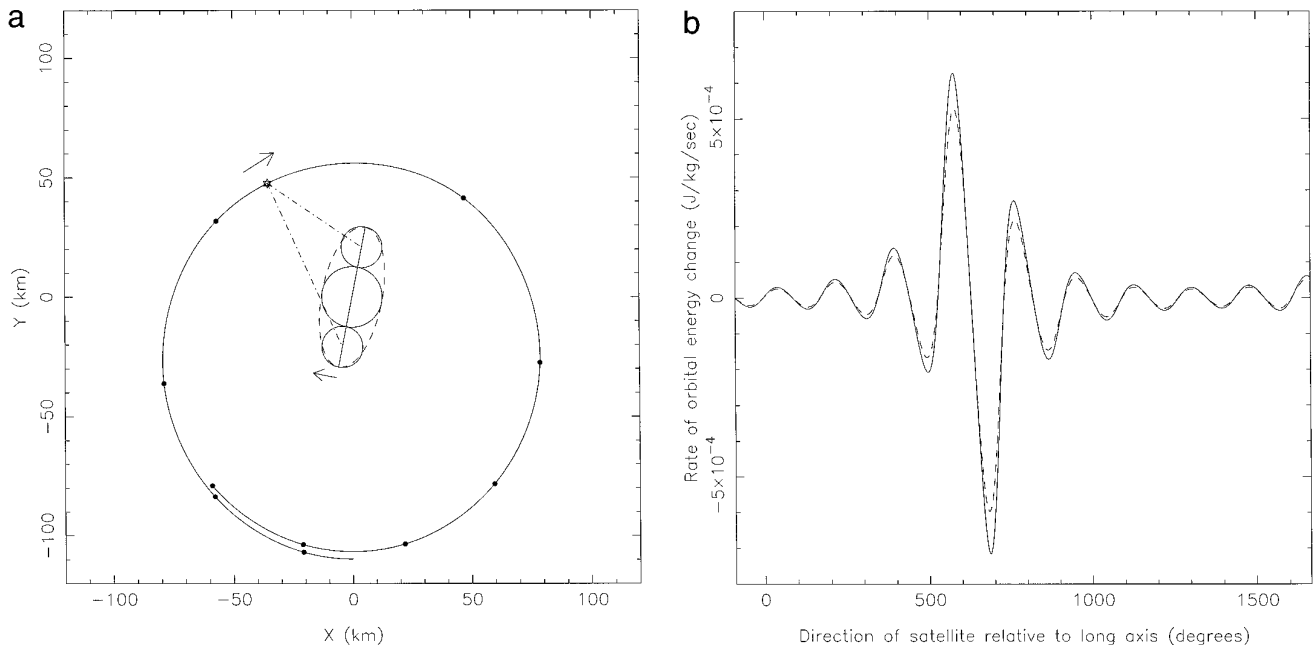


**FIG. 12.** (a) A 5:1 commensurable prograde orbit plotted in an inertial frame. Dots indicate the position of the satellite when it is aligned with the primary's long axis. The open star indicates the satellite position when it is at  $45^\circ$  off the short axis before passage at pericenter. The solid straight line through the focus of the orbit is the long axis of the primary at that time. Dash-dotted lines indicate the orientation of the perturbing forces on the satellite. The dashed ellipse shows the best fit ellipsoid to Ida's figure and the solid circles represent the three-sphere model. (b) Rate of orbital energy change (for the three-sphere model, solid curve, and a similar ellipsoid, dashed line). If (as in the case shown) pericenter does not occur when the satellite is aligned with an axis of symmetry of the primary, the curve is asymmetrical and a net energy change is accumulated. The corresponding change in orbital period tends to keep pericenter away from the long axis.

#### D. Characterizing Resonances by a Hamiltonian Approach

To precisely determine the orbital elements, for a zero-libration, stable commensurable orbit in the Galileo family, we adopt a formal Hamiltonian approach. We derive a representation of the system in terms of “actions” and “angles.” For a resonant orbit, one of the angles and its conjugate action do not evolve. Hence, the Hamiltonian has an extremum value with respect to these variables at the resonance. We introduce the Delaunay variables

$$\begin{aligned}
 l &= \text{mean anomaly,} \\
 L &= \sqrt{\mu a}, \\
 g &= \text{argument of pericenter,} \\
 G &= \sqrt{\mu a(1 - e^2)}, \\
 h &= \text{longitude of node,} \\
 H &= G \cos(i),
 \end{aligned} \tag{1}$$

where  $i$  is the inclination of the orbit, and the longitude,  $h$ , is measured from the body-fixed zero longitude on Ida (i.e., from the end of Ida's long axis). Here and in the

following, the capital letters represent action variables, while lowercase letters stand for the conjugate angle variable. The Hamiltonian is

$$\mathcal{H} = -\frac{\mu^2}{2L^2} - \omega H + U_{\text{pert}}(x, y, z), \tag{2}$$

where  $\mu$  is the product of the mass of Ida and the gravitational constant,  $\omega$  is the rotational frequency of Ida, and  $U_{\text{pert}}(x, y, z)$  is the perturbation potential, e.g., the difference between the true potential and the potential generated by a point with the same mass as the primary and located in its center of mass.  $x, y, z$  are Cartesian coordinates in the Ida-fixed rotating frame, and

$$\begin{aligned}
 \mu x &= \left[ \cos(h) \cos(g) - \frac{H}{G} \sin(h) \sin(g) \right] L^2 (\cos(E) - e) \\
 &\quad + \left[ -\cos(h) \sin(g) - \frac{H}{G} \sin(h) \cos(g) \right] GL \sin(E), \\
 \mu y &= \left[ \sin(h) \cos(g) + \frac{H}{G} \cos(h) \sin(g) \right] L^2 (\cos(E) - e)
 \end{aligned}$$

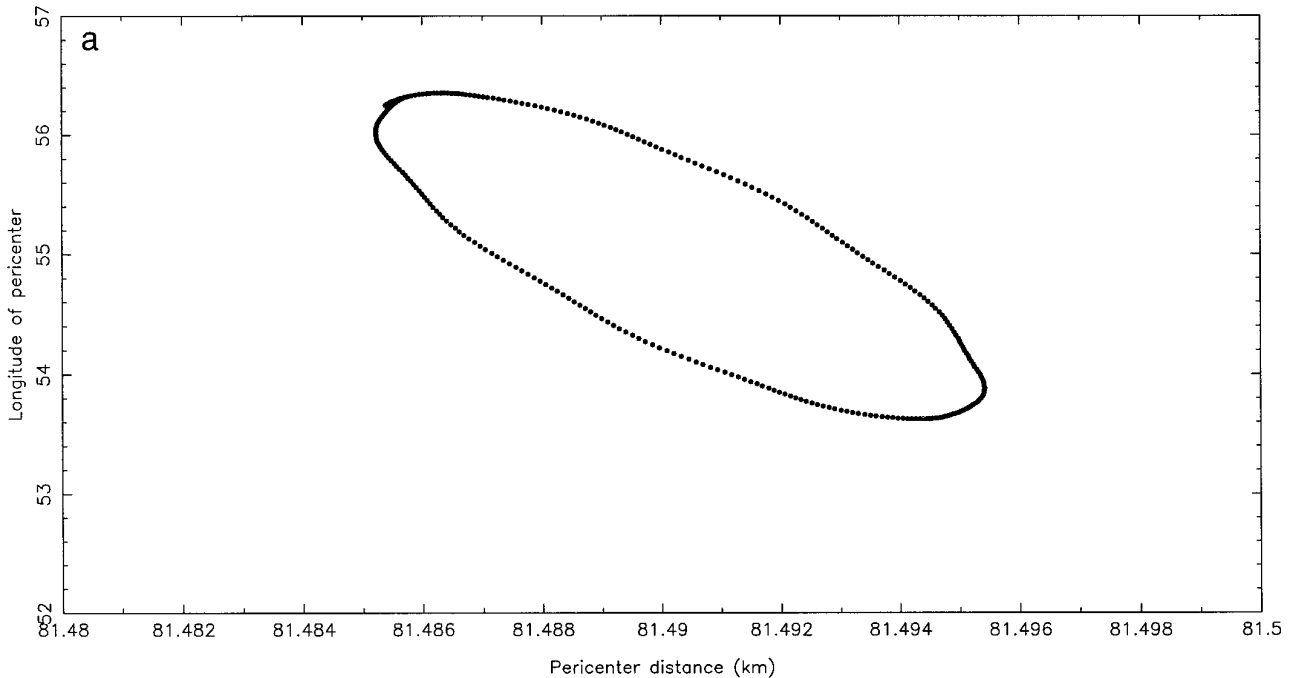


**FIG. 13.** (a) Pericenter for a 6:1 commensurability is locked to a longitude near  $55^\circ$  relative to Ida's long axis. Such stable commensurabilities generally lock pericenter to the convex side of Ida, not the opposite (concave) side. The wiggles are due to out-of-plane oscillations which remain  $\leq 1^\circ$ . (b) Pericenter for an 11:2 commensurability alternates between two different Ida-centric longitudes on opposite sides of Ida, but both near  $90^\circ$  from the long axis. Pericenter is locked to these longitudes. As in (a), the small wiggles are due to the small, variable inclination of the orbit.

$$\begin{aligned} & + \left[ -\sin(h)\sin(g) + \frac{H}{G}\cos(h)\cos(g) \right] GL \sin(E), \\ \mu z = & \sqrt{1 - \frac{H^2}{G^2}} (\sin(g)L^2(\cos(E) - e) + \cos(g)GL \sin(E)). \end{aligned} \quad (3)$$

Also,

$$E - e \sin(E) = l, \quad (4)$$

$E$  being the eccentric anomaly.

To reduce the number of dimensions and make the problem computationally tractable, we restrict ourselves to orbits lying in the equatorial plane, e.g.,  $i = 0^\circ$ . To be sure that an orbit starting in the equatorial plane will remain in this plane, we use a shape model symmetric with respect to the  $(x, y)$  plane. This symmetrical shape model is constructed by reflecting the 44-sphere model about the equatorial plane, and dividing the mass of each sphere by 2, creating an 88-point-mass model. In the  $(x, y)$  plane, the potential field of this model is the same as in the 44-sphere model, within the uncertainties of the true gravitational figure. Also, results that we obtain are consistent with numerical integrations described in Sections IIIA and B.

With  $i \equiv 0^\circ$ , the dimensionality of the problem is reduced

because  $H \equiv G$ , and  $g$  and  $h$  are undefined, but the longitude of pericenter ( $g + h$ ) is well defined. Also, because we are interested in  $p:q$  commensurabilities between the orbital period and the rotational period of the primary (here,  $q$  is an integer, e.g.,  $p = 5$ ,  $q = 1$ ), the angle  $-(p/q)l - (g + h)$  is constant, or slowly varying. (Remember, by definition,  $g + h$  is the longitude of pericenter, which is usually written  $\tilde{\omega}$ , measured relative to the body-fixed prime meridian on Ida.) So we introduce a canonical change of variables:

$$\begin{aligned} \sigma &= \frac{-p}{Nq}l - (g + h), \\ S &= -H, \\ n &= l, \\ N &= L - \frac{p}{q}H. \end{aligned} \quad (5)$$

When we are close to a  $p:q$  commensurability,  $n$  varies rapidly compared with  $\sigma$ . So we look at the averaged Hamiltonian

$$\overline{\mathcal{H}} = \frac{1}{2\pi q} \int_0^{2\pi q} \mathcal{H} dn. \quad (6)$$

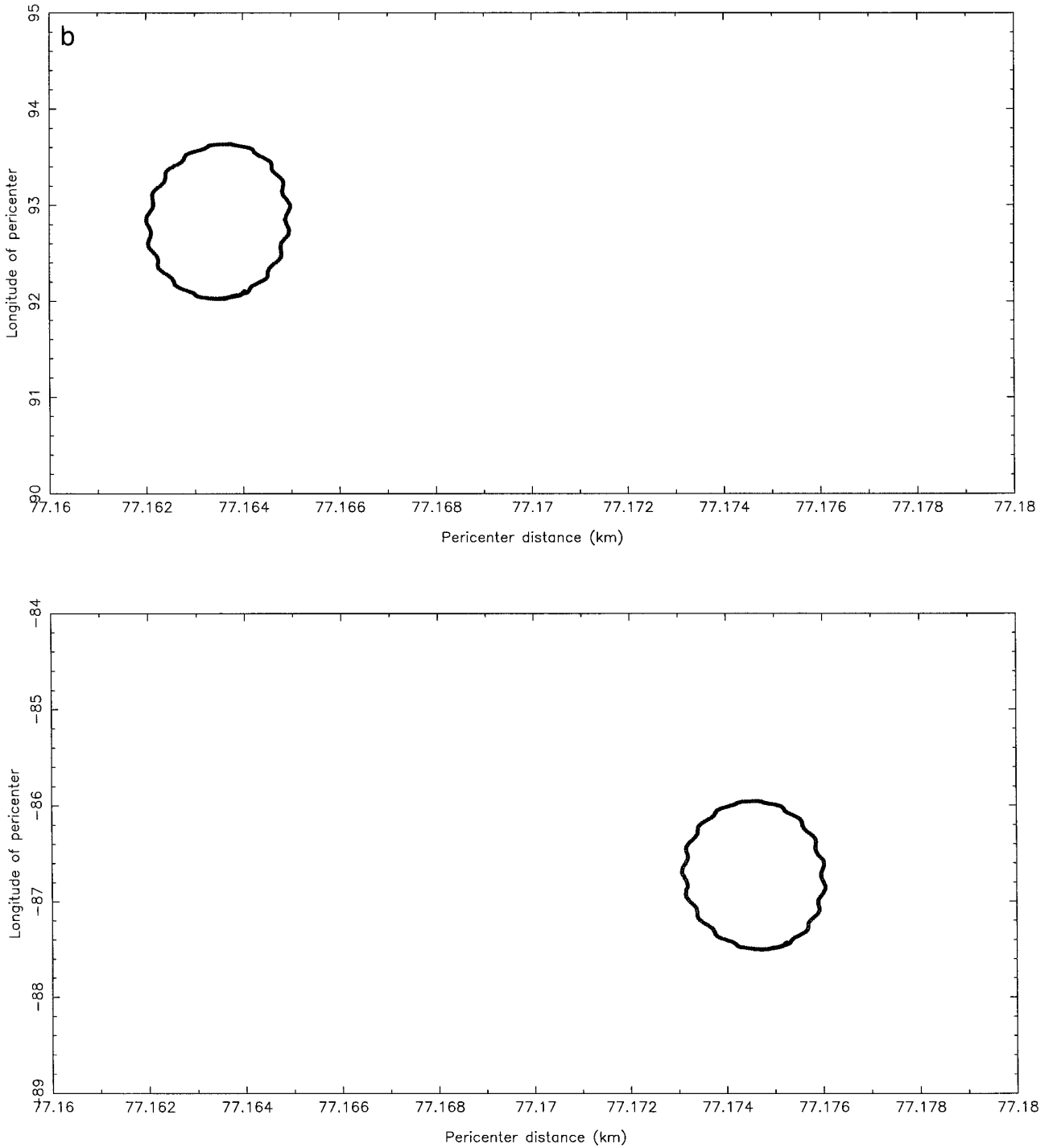


FIG. 13—Continued

The averaged Hamiltonian  $\overline{\mathcal{H}}$  no longer depends on  $n$ , the mean anomaly. Remember that  $n$  and  $N$  are conjugate variables and  $\dot{n} = \partial\overline{\mathcal{H}}/\partial N$  and  $\dot{N} = \partial\overline{\mathcal{H}}/\partial n$ . Hence  $N$  is a constant of motion and can be considered as a parameter. Only two variables are left,  $S$  and  $\sigma$ .

To find equilibrium conditions, we look for extrema of

the surface  $\overline{\mathcal{H}}(S, \sigma)$ . For a given value of Ida's mass, we have a corresponding orbital period from the Galileo family of fit orbits. We take the order of commensurability  $p:q$  (with  $q = 1$  or  $2$ ) as being the ratio closest to the fit orbit's orbital period divided by the rotational period of Ida. Then we consider a range of values for  $N$ , and

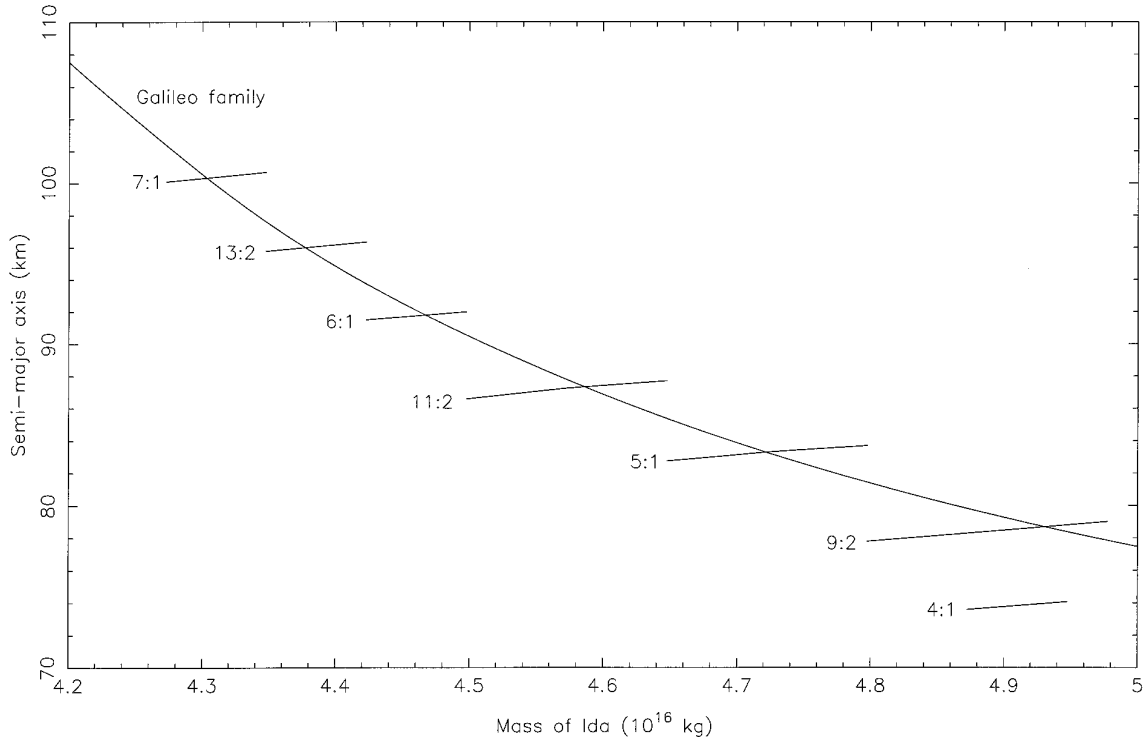


FIG. 14. Comparison between Galileo family orbits and  $p:q$  commensurable orbits. The commensurable orbits shown have the eccentricity of the Galileo orbit with the same mass of Ida. Where curves cross, we have Galileo family orbits that are in stable commensurabilities.

for each of these values, we look for the extremum of  $\overline{\mathcal{H}}(S, \sigma)$ . The values of  $N$  and  $S$  at that point give  $a$  and  $e$  for an exactly resonant orbit for that particular mass of Ida. For example, a contour plot of  $\overline{\mathcal{H}}(S, \sigma)$  is shown in Fig. 17 for the case with  $p = 5$ ,  $q = 1$ ,  $M = 4.72 \times 10^{16}$  kg ( $\mu = 0.00315$  km<sup>3</sup> sec<sup>-2</sup>), and  $N = -2020250$  m<sup>2</sup> sec<sup>-1</sup>. The extremum at  $S = -506,605$  m<sup>2</sup> sec<sup>-1</sup> at point A is the stable resonance. This point corresponds to  $a = 83.47$  km and  $e = 0.155$ . Note that there is only one allowed orientation of the pericenter for a resonant orbit, on one side of the primary, not two as there would be for a symmetrical primary.

TABLE I  
Dactyl's Ida-centric Longitude of Pericenter for Low-Order Commensurabilities Compared with Galileo Data

Commensurability	$M$ ( $10^{16}$ kg)	$\rho$ ( $\text{g cm}^{-3}$ )	Stable longitude (deg)	Observed longitude (deg)
7:1	4.30	2.67	50.4	90.0
13:2	4.38	2.72	92.9/-86.8	151.2
6:1	4.47	2.78	55.0	-103.6
11:2	4.59	2.85	92.8/-87.7	30.3
5:1	4.72	2.93	76.5	92.8
9:2	4.93	3.06	93.7/-87.5	73.3

The function  $\overline{\mathcal{H}}(S, \sigma)$  also can be used to define the width of the resonance zone, i.e., the width of the well that contains the exact resonance point. For example, the saddle point (B) in Fig. 17 represents the limiting value of  $\overline{\mathcal{H}}$  for resonant libration. The contours passing through point B form a separatrix bounding the resonance zone, which can equivalently be mapped into  $(a, e)$  space.

Thus for any value of assumed mass of Ida, we can generate a curved line in  $(a, e)$  space that represents the locus of zero libration for all possible values of  $N$ , and around that line are the boundaries of maximum libration. We have followed that procedure over the range of values of  $M$  corresponding to the Galileo family of orbits. Specifically, we repeated this procedure for all values of  $\mu$  from 0.00330 to 0.00240 km<sup>3</sup> sec<sup>-2</sup> in increments of 0.00001 km<sup>3</sup> sec<sup>-2</sup> (masses from  $4.95 \times 10^{16}$  to  $3.6 \times 10^{16}$  kg in increments of  $0.015 \times 10^{16}$  kg). We used a spline fit to the published Galileo family parameters to obtain the  $(a, e)$  values corresponding to each  $M$ . (The increment corresponds to steps in  $a$  of  $\sim 0.5$  km, for Ida densities of 2.5 to 3.0 g cm<sup>-3</sup>.) Results are plotted in Fig. 18. For each commensurability ( $p:1$  or  $p:2$ ) there is, in principle, a curve in  $(a, e)$  space for each  $M$  value over some range of  $M$  values. However, in Fig. 18, we plot only the commensurability curve that includes  $(a, e)$  values closest to the corresponding  $(a, e)$  values from the Galileo family. In this way



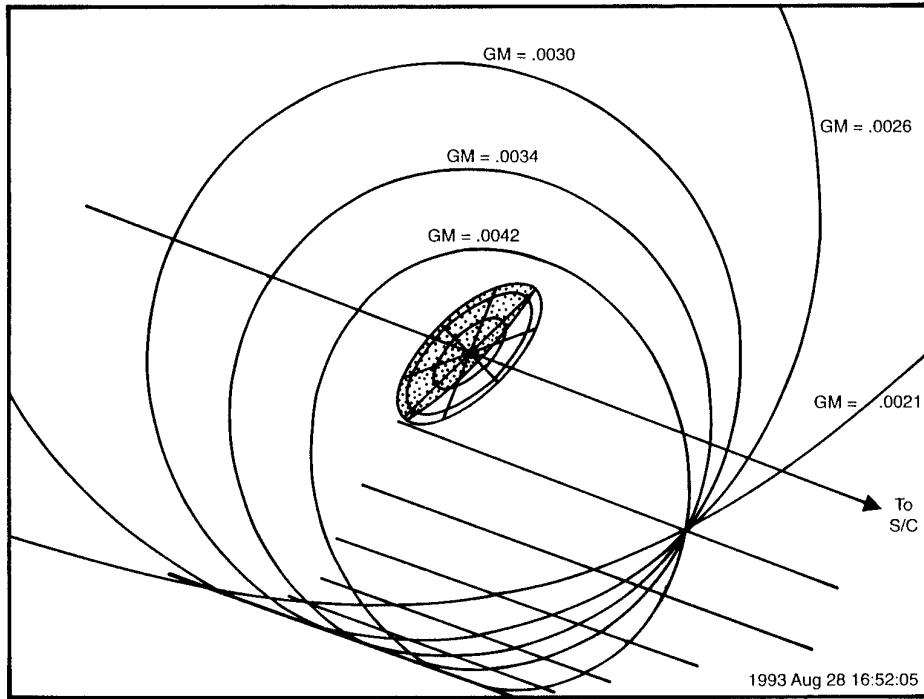


FIG. 15. Possible fit orbits of Dactyl for different values of parameter  $GM$ . The central ellipse shows the orientation of Ida at epoch 28 August 1993 16:52:05 UT, Dactyl being located at the intersection of all orbits. The arrows point toward the spacecraft. Reproduced, with permission, from Belton *et al.* (1995).

we identify the members of the Galileo family of orbits that are at stable commensurabilities (or at least near them, given the incremental process). In Fig. 18, these orbits are at the intersections of the commensurability curves with the Galileo family curve. Figure 18 shows the results for the range of Ida masses from  $M = 4.25 \times 10^{16}$  to  $5.0 \times 10^{16}$  kg (density 2.6 to 3.1  $\text{g cm}^{-3}$ ), within the zone of stability (as shown in Fig. 6).

The width of the resonance zones given in Fig. 18 shows that it is more likely for a satellite to be trapped in the 5:1 or 9:2 resonance than the other low-order resonances. For example, for the 7:1 case the width is of the order of 200 m. In the case of the 9:2 resonance, the width is 2 km.

In Fig. 19, we show results for  $M = 3.6 \times 10^{16}$  kg (density 2.24  $\text{g cm}^{-3}$ ). Note that the resonances overlap for values of  $e$  very close to the Galileo family (black dot). Even minimal libration can thus lead to chaotic behavior. The boundary for  $q < 65$  km is located nearby (dotted line), so that chaotic behavior can cause the orbit to go into that unstable zone of small  $q$ . This explains the boundaries of chaotic behavior at  $M = 4.0 \times 10^{16}$  kg ( $a = 127$  km) and of instability at  $M = 3.65 \times 10^{16}$  ( $a = 244$  km) in Fig. 6.

In contrast, for the range of orbits shown in Fig. 18, the resonances are well spaced, with no evident mechanism for chaos.

In all these simulations, we have neglected the solar

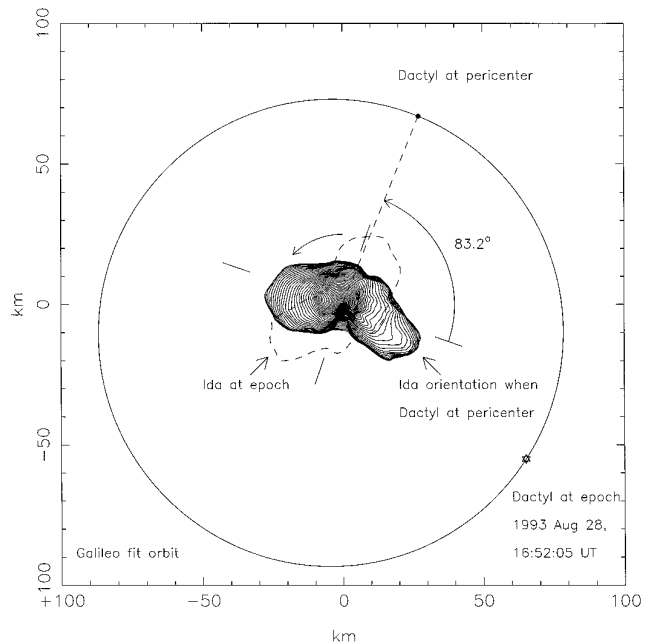


FIG. 16. Advancing Dactyl forward from its observed position at epoch to pericenter (on the 5:1 orbit that is in the Galileo family) gives the Ida-centric longitude of pericenter shown in Table I.

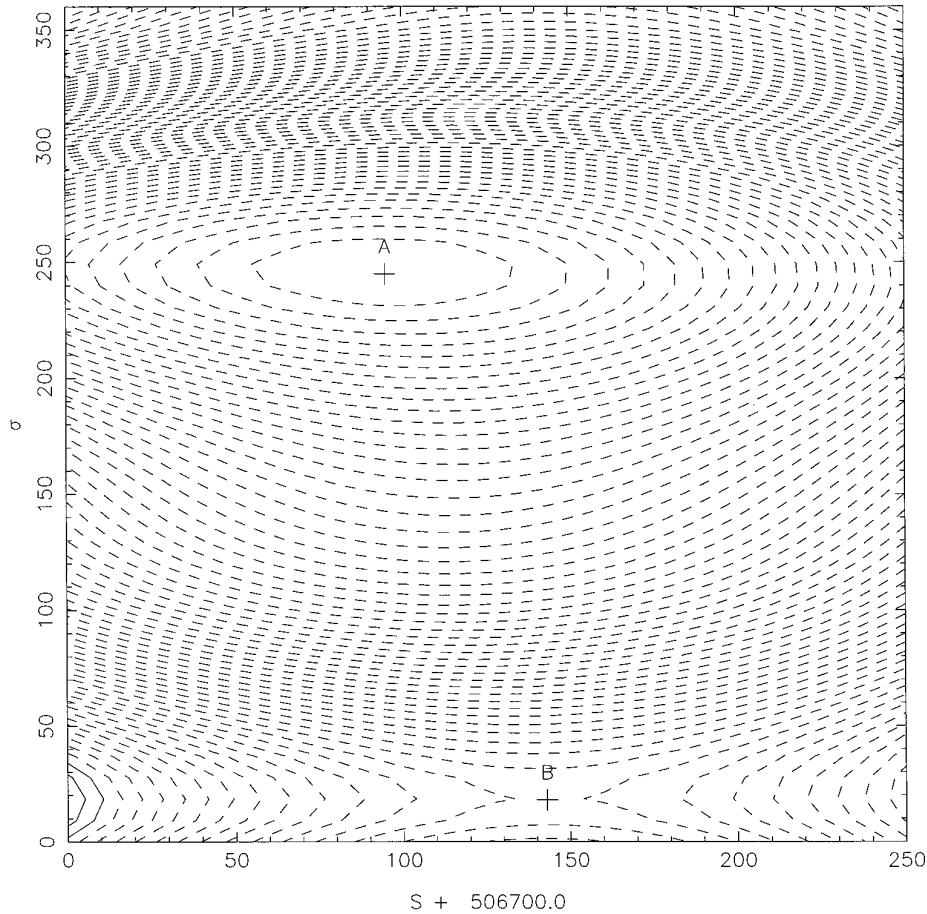


FIG. 17. Contour plot of the averaged Hamiltonian as a function of  $S$  and  $\sigma$  for  $N = -2020250 \text{ m}^2 \text{ sec}^{-1}$  and  $p:q = 5:1$ . Point A denotes the extremum point, and point B the saddle point.

perturbations. For the orbits shown in Fig. 18, this is not a problem since the satellite always stays very close to Ida. For the orbit shown in Fig. 19, the apocenter distance reaches several hundred kilometers. This is still well within the Hill radius of about 10,000 km. Solar perturbations are then very small and act on time scales longer than 1000 years, which is the typical time scale for chaos and escape for these orbits.

### E. Long-Term Stability of Resonant Orbits

Next we consider whether these resonant orbits are any more stable over long time scales than nearby, non-commensurate orbits. To address this question we have performed a series of very long time scale (thousands of years) numerical integrations of the 5:1 orbit and neighboring non-resonant orbits as an example. As in the previous section, orbits started with zero inclination (e.g., in the equatorial plane of Ida) but with the same other osculating elements as the Galileo family. We find that the time evolution of the Lyapunov characteristic indicator (defined in

the Appendix) for the 5:1 resonance is very similar to the one shown in Fig. 9. The logarithm of the Lyapunov indicator decreases linearly with logarithm of time for at least 6000 years, indicating a stable, non-chaotic orbit. The nearby, non-resonant orbits have Lyapunov characteristic indicators that are qualitatively indistinguishable from the 5:1 commensurability one, showing that these orbits are just as stable. Thus these preliminary results indicate that resonant orbits offer no significant advantage over other orbits in stabilizing Dactyl over thousands of years.

These results are only preliminary because we need to understand stability over tens of millions of years, which is Dactyl's likely lifetime. We also need to investigate the relative stability of the other commensurabilities as well.

We have considered only the so-called eccentricity resonances, which ensure that at pericenter, the satellite will always be aligned with a given axis, avoiding close encounters with the ends of Ida. Inclination resonances, by locking the node position, will not have such a protection mechanism. Preliminary integrations with dissipative forces show

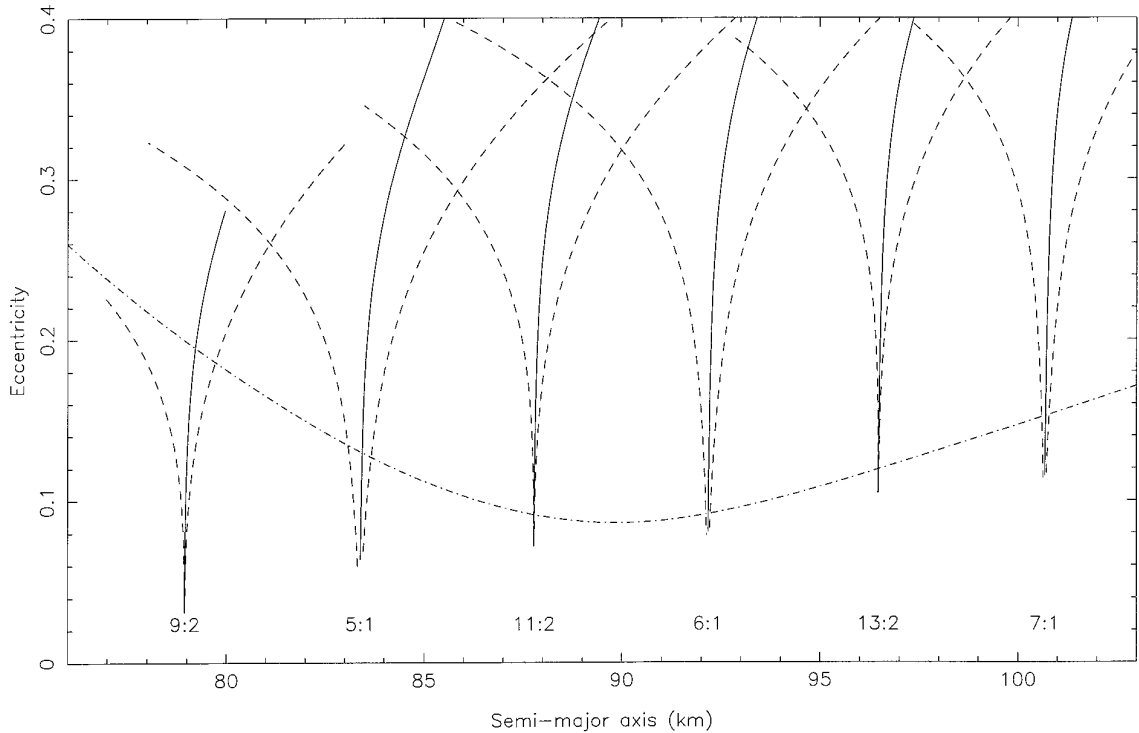


FIG. 18. Location of resonant orbits in the  $(a, e)$  plane. Solid lines represent the commensurabilities, the dashed lines limit the regions of librating orbits, and the dash-dotted line shows the Galileo family of orbits for a range of masses of Ida. Resonances are plotted for the masses of Ida where they fit the Galileo family.

that the orbit is indeed trapped into these eccentricity resonances. All other resonances may act on time scales longer than the 6000 years considered here.

#### IV. CONCLUSIONS

Dactyl's orbit probably lies fairly close to orbits that would be unstable on very short time scales. Fundamentally, such instability is due to the very elongated figure of Ida and its proximity to Dactyl. The original indication came from our study of orbits around a triaxial ellipse with parameters similar to Ida's. We found that the dominant criterion for instability was the distance of pericenter from Ida: If it was less than about 65 km, for a direct orbit like Dactyl's, the satellite soon impacts the primary or is ejected. The family of orbits that fit Galileo images includes a broad range with lower pericenter distances. These orbits correspond to assumed densities of Ida greater than about  $3 \text{ g cm}^{-3}$ .

Refinement of that result has been done by numerically integrating motion around a primary with a figure close to the actual figure of Ida. Orbits in the Galileo family were explored, demonstrating that those with densities greater than  $3.1 \text{ g cm}^{-3}$  were unstable on time scales of days to

months. Moreover, at the opposite extreme of density, orbits corresponding to densities less than  $2.3 \text{ g cm}^{-3}$  are chaotic and become unstable after about 1000 years, usually because the pericenter dips below the critical distance from Ida. For density between  $2.3$  and  $2.5 \text{ g cm}^{-3}$ , Galileo family orbits are chaotic but there is no indication of instability over thousands of years.

Dactyl is probably at least tens of millions of years old, so its orbit must be stable over time scales much longer than we have been able to explore numerically. We have investigated the character of commensurate orbits within the Galileo family. First, with the ellipsoidal-primary model, we showed how orbits commensurate with the rotation of Ida are stabilized by interactions with the long-axis bulges of the elongated primary. Then we explored the character and stability of  $p:1$  and  $p:2$  resonances with realistic Ida models. These resonances are stable. If we could show that one or some of these orbits were particularly stable over the long term, or otherwise favorable, we could constrain the mass and density of Ida to the corresponding value. In fact, however, all low-order cases are consistent with the longitudinal position of Dactyl at the epoch of the Galileo encounter, and there is no evidence of preferential stability against collision with Ida or escape over the time

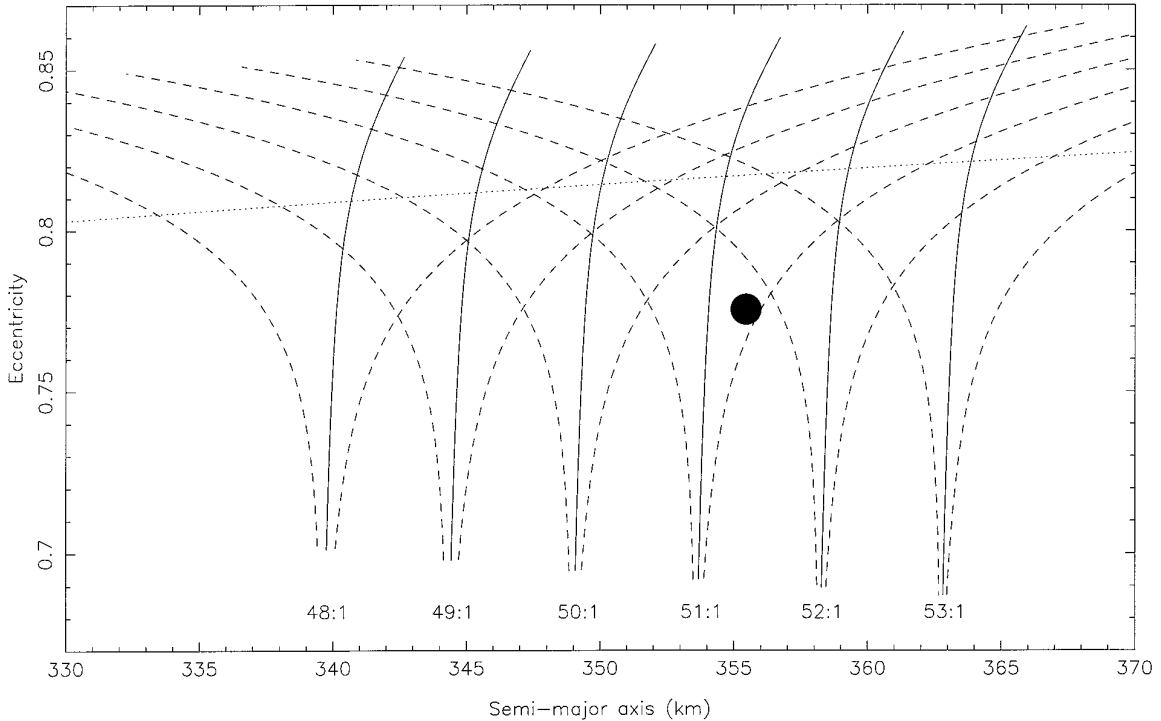


FIG. 19. Similar to Fig. 18, except all resonances assume the same mass ( $M = 3.6 \times 10^{16}$  kg, as an example). The Galileo family ( $a, e$ ) for this mass is shown by the black dot. The orbit is close to where resonances overlap (chaos), which can lead to crossing the dashed line (pericenter of 65 km) and instability.

scales we have investigated. Perhaps future integrations over longer times will show some preference for the resonant orbits.

Another process that may have favored resonant orbits may have been orbital evolution due to dissipative effects, such as collisional drag. As Dactyl orbits Ida it also passes through a variable cloud of impact-generated orbital debris, lofted into temporary trajectories about Ida after large cratering impacts (Geissler *et al.* 1996). Passage through this debris creates a small drag on the satellite, causing its orbit about Ida to slowly decay. Collisions from dust and small particles from the asteroidal belt cause the same kind of drag. Regardless of Dactyl's provenance, it may have since been captured into a stable resonant orbit after evolving inward toward Ida due to debris-induced drag. Preliminary study of the evolution of the semimajor axis of an Ida satellite near a resonance under the influence of a gas-drag-like force shows that the orbit decays at a steady rate until captured into the resonance. As is typical in a resonance with an induced drag force, the eccentricity of the orbit slowly increases until the satellite enters a secondary resonance overlapping the primary one (Henrard and Moons 1992). The orbit then evolves along this secondary resonance on a chaotic path. Eventually, it crosses the separatrix of the primary resonance and continues to

evolve inward. Therefore, a satellite evolving under dissipative forces may be trapped temporarily and sequentially into resonances and may stay in each for geological times, thus favoring discovery in resonance at any particular epoch. Another dissipative effect we must consider is due to tides raised on Ida by Dactyl. To conduct this study, we cannot use standard tidal dissipation formulas due to the odd shape of Ida. Further work on this problem is underway.

## APPENDIX

The Lyapunov characteristic number (LCN, Benettin *et al.* 1980, Froeschlé 1984) characterizes the divergence rate of two neighboring orbits. Let us consider a differential equation:

$$\frac{dX}{dt}(t) = F(X, t). \quad (\text{A1})$$

We want to know how the point  $X(t) + \varepsilon(t)$  diverges from  $X(t)$ , where  $\varepsilon(t)$  is a small quantity. We expand Eq. (A1) to find the equation governing the evolution of  $\varepsilon(t)$ ,

$$\frac{dX}{dt}(t) + \frac{d\varepsilon}{dt}(t) = F(X + \varepsilon, t) = F(X, t) + L_{(X,t)} \cdot \varepsilon + O(\varepsilon^2), \quad (\text{A2})$$

where  $L_{(X,t)}$  is the Jacobian matrix at point  $X$  and time  $t$ . Since  $\varepsilon$  is

an infinitely small vector, its evolution is governed by the well-known variation equation

$$\frac{d\varepsilon}{dt}(t) = L_{(x,t)} \cdot \varepsilon. \quad (\text{A3})$$

This is a linear equation, so we can normalize  $\varepsilon$  as we wish. It is well known that the quantity

$$\Gamma(\varepsilon(0), T) = \frac{1}{T} \frac{\|\varepsilon(T)\|}{\|\varepsilon(0)\|} \quad (\text{A4})$$

is independent of  $\varepsilon(0)$  and tends to a limit, which is the largest LCN, as  $T$  goes to infinity. A strictly positive LCN means that two neighboring points will diverge exponentially in time, which formally defines chaotic motion. In practice, we define the Lyapunov characteristic indicators as the truncated values of the LCNs for a finite time and we use these to determine chaotic behavior.

### ACKNOWLEDGMENTS

This work was supported by NASA Grant NAGW-1029 and by CNRS. We thank Doug Hamilton and an anonymous referee for their constructive reviews. We are grateful to D. Byrnes and L. D'Amario for sharing with us their data on orbital determination, and to D. Scheeres and A. Morbidelli for interesting discussions. We thank the Galileo project and Galileo imaging team for obtaining these remarkable data.

### REFERENCES

Belton, M. J. S., and R. Carlson, 1994. *1993 (243)1*. IAU Circ. 5948.  
 Belton, M., C. Chapman, P. Thomas, M. Davies, R. Greenberg, K. Klaasen, D. Byrnes, L. D'Amario, S. Synnott, W. Merline, J-M. Petit, A. Storrs, B. Zellner, and the Galileo Imaging Team 1995. The bulk density of asteroid 243 Ida from Dactyl's orbit. *Nature* **374**, 785–788.  
 Belton, M., B. Mueller, L. D'Amario, D. Byrnes, K. Klaasen, S. Synnott, H. Breneman, T. Johnson, P. Thomas, J. Veverka, A. Harch, M. Davies,

W. Merline, C. Chapman, D. Davis, T. Denk, J-M. Petit, R. Greenberg, A. McEwen, A. Storrs, and B. Zellner 1996. The discovery and orbit of 1993 (243) 1 Dactyl. *Icarus* **120**, 185–199.  
 Benettin, G. L., A. Giorgilli, and J. M. Strelcyn 1980. *Meccanica* **15**, 10.  
 Byrnes, D., and L. D'Amario 1994. Galileo Imaging Team Report, unpublished.  
 Chauvineau, B., P. Farinella, and F. Mignard 1993. Planar orbits about a triaxial body: Application to asteroidal satellites. *Icarus* **105**, 370–384.  
 Durda, D. D. 1993. *The Collisional Evolution of the Asteroid Belt and Its Contribution to the Zodiacal Cloud*. Ph.D. thesis, Univ. of Florida.  
 Durda, D. D. 1996. The formation of asteroidal satellites in catastrophic collisions. *Icarus* **120**, 212–219.  
 Durda, D. D., and P. Geissler 1996. The formation of asteroidal satellites in large cratering collisions. *Bull. Am. Astron. Soc.* **28**, 1101.  
 Froeschlé, C. 1984. Numéro spécial du journal de Mécanique théorique et appliquée 101.  
 Geissler, P., J-M. Petit, D. D. Durda, R. Greenberg, W. Bottke, M. Nolan, and J. Moore 1996. Erosion and ejecta redistribution on 243 Ida and its moon. *Icarus* **120**, 140–157.  
 Greenberg, R., W. Bottke, M. Nolan, P. Geissler, J-M. Petit, D. D. Durda, E. Asphaug, and J. Head 1996. Collisional and dynamical history of Ida. *Icarus* **120**, 106–118.  
 Henrard, J., and M. Moons 1992. Capture probabilities for secondary resonances. *Icarus* **95**, 244–252.  
 Hurford, T., D. D. Durda, R. Greenberg, J-M. Petit, P. Geissler, and W. Bottke 1995. Stable periodic orbits around Ida: Several fit Dactyl's motion. *Bull. Am. Astron. Soc.* **27**, 1070–1071.  
 Laskar, J. 1990. The chaotic motion of the Solar System: A numerical estimate of the size of the chaotic zones. *Icarus* **88**, 266–291.  
 Petit, J-M., R. Greenberg, and P. Geissler 1994. Orbits around a small, highly elongated asteroid: Constraints on Ida's Moon. *Bull. Am. Astron. Soc.* **26**, 1157–1158.  
 Scheeres, D. 1994. Dynamics about uniformly rotating triaxial ellipsoids: Application to asteroids. *Icarus* **110**, 225–238.  
 Scheeres, D. J., S. J. Ostro, R. S. Hudson, and R. A. Werner 1996. Orbits close to asteroid 4769 Castalia. *Icarus* **121**, 67–87.  
 Thomas, P., M. Belton, B. Carcich, C. Chapman, M. Davies, R. Sullivan, and J. Veverka 1996. The shape of Ida. *Icarus* **120**, 20–30.